Research Article

Shuguang Li, Nainaru Tarakaramu, Muhammad Ijaz Khan*, Narsu Sivakumar, Panyam Venkata Satya Narayana, Sherzod Abdullaev, Nissren Tamam, and Sayed M. Eldin

Enhanced heat transfer and fluid motion in 3D nanofluid with anisotropic slip and magnetic field

https://doi.org/10.1515/phys-2023-0131
received July 01, 2023; accepted October 12, 2023

Abstract: A mathematical model is envisaged that discusses the motion of 3D nanofluids (NFs) with anisotropic slip influence magnetic field past a stretching sheet. The heat transportation phenomenon is analysed by melting effect, heat generation, and chemical reaction. The main motivation of this study is to analyse the behaviour of liquid motion and heat transfer (HT) of NFs because this study has huge applications in boiling, solar energy, and micropower generation, which are used in the engineering process. The physical governing partial differential equation is transformed into a coupled non-linear system of ordinary differential equations using suitable appropriate transformations. The translated equations are calculated using Runge–Kutta–Fehlberg method *via* shooting procedure. The physical characteristics of various parameters on velocities, concentration, and thermal fields are explored in detail. The HT is high in NFs when compared to pure or regular liquids for ascending values of heat source parameter and slip factor. Also, the skin friction coefficients *via* coordinate axes and rate of Nusselt number were analysed.

Keywords: melting effect, nanofluid, MHD, heat source, chemical reaction, slip condition, thermal radiation

*** Corresponding author: Muhammad Ijaz Khan,** Department of Mathematics and Statistics, Riphah International University I-14, Islamabad, 44000, Pakistan; Department of Mechanical Engineering, Lebanese American University, Kraytem, 1102-2801, Beirut, Lebanon, e-mail: scientificresearchglobe@gmail.com
Shuguang Li: School of Computer Science and Technology, Shandong Technology and Business University, Yantai, 264005, China
Nainaru Tarakaramu: Department of Mathematics, School of Liberal Arts and Sciences, Mohan Babu University, Sree Sainath Nagar, Tirupati, 517102, A.P., India; Department of Mathematics, Basic Sciences and Humanities, Sree Vidyanikethan Engineering College, Sree Sainath Nagar, Tirupati, 517102, A.P., India
Narsu Sivakumar: Department of Mathematics, College of Engineering and Technology, SRM Institute of Science and Technology, Kattankuluthur, Chennai, 603203, T.N., India
Panyam Venkata Satya Narayana: Department of Mathematics, School of Advanced Sciences, Vellore Institute of Technology, Vellore, 632 014, T.N., India
Sherzod Abdullaev: Faculty of Chemical Engineering, New Uzbekistan University, Tashkent, Uzbekistan; Department of Science and Innovation, Tashkent State Pedagogical University Named After Nizami, Bunyodkor Street 27, Tashkent, Uzbekistan
Nissren Tamam: Department of Physics, College of Science, Princess Nourah bint Abdulrahman University, P.O. Box 84428, Riyadh, 11671, Saudi Arabia
Sayed M. Eldin: Center of Research, Faculty of Engineering, Future University in Egypt, New Cairo, 11835, Egypt

Nomenclature

(x_1, y_1)	Cartesian coordinates
u_1, u_2, and u_3	velocity components along x_1, y_1, z_1-axis
C_1	volume fraction of nanoparticle
C_f	skin friction coefficient
c_p	specific heat
C_∞	uniform ambient concentration
D_B	Brownian diffusion
D_T	thermophoresis diffusion
f	dimensionless stream function
f'	dimensionless velocity
H	heat source parameter $=Q_0/a_1(\rho c_p)$
k_1	thermal conductivity
Le	Lewis number $=\alpha_1/D_B$
M	magnetic field parameter $=\frac{\sigma_1 B_0^2}{a_1\rho_f}$
Mt	melting parameter $\frac{c_f(T_\infty - T_m)}{\lambda_1 + c_s(T_m - T_s)}$
N_t	thermophoresis parameter $=\frac{\tau_1 D_T}{\alpha_1 T_\infty}(T_W - T_\infty)$
N_b	Brownian motion coefficient $=\frac{D_B\tau_1(C_W - C_\infty)}{\alpha_1 \upsilon_1}$
Pr	Prandtl number $=\left(\frac{\upsilon_1}{\alpha_1}\right)$
q_r	radiative heat flux
Re_x	Reynolds number
R_d	radiation parameter $=\frac{16\sigma_1 T_\infty^3}{3(\rho c_p)\alpha_1 k_1}$
T_1	temperature of the fluid

T_s	solid surface temperature
T_m	temperature of the melting surface
T_∞	fluid temperature far away from the surface
T_w	constant fluid temperature of the wall
U_w	stretching velocity
U_∞	free stream velocity

Greek symbols

μ_1	dynamic viscosity
ϕ	dimensionless concentration
σ_1	Boltzmann's constant
γ	chemical reaction parameter $=k_0/a_1$
λ_1	slip factors $=N_i\mu_1\sqrt{a_1/\upsilon_1}$
υ_1	kinematic viscosity of the fluid
α_1	thermal diffusivity $=k_1/(\rho c_p)$
τ_1	ratio of the nanoparticle to the fluid $(\rho c)_p/(\rho c)_f$
$(\rho c)_f$	heat capacity of the fluid
$(\rho c)_p$	heat capacity of the nanoparticle to the fluid
ρ	density

Subscripts

∞	condition at free stream

Abbreviation

HT	heat transfer
TR	thermal radiation
TD	thermal diffusivity
3D	three-dimensional
CR	chemical reaction
MT	melting transfer
BL	boundary layer
HGT	homogenous reaction
NFs	nanofluids
HTM	heat and mass transfer
MHD	magnetohydrodynamic
SS	stretching sheet
2D	two-dimensional
RFs	regular fluids
CLAM	China low activation martensitic
HR	heterogeneous reaction

1 Introduction

The melting transfer is more popular topic in upcoming researchers because it is closely related to a wide range of technologically significant processes. The impact of melting (fusion) is a physical process (phase conversion of a material from a solid to a fluid). It has various natural applications of heat or pressure (such as thermocouples, semiconducting materials, storage of latent heat, sanitization, optical material processing, permafrost melting, crystal growth, heat transfer (HT) and heat engines, metal casting, glass industry, solidifying magma, defrosting in frozen grounds, freezing of soil around the heat exchanger coils of a thermal energy storage, ground-based pump), laser manufacturing (drilling welding and selective sintering), *etc.* Epstein and Cho [1] examined the exact solutions for melting motion of HT *via* flat plate. On the other hand, Kamierczak *et al.* [2,3] studied melting of a vertical flat plate *via* porous medium with convection motion. Rahman *et al.* [4] presented the melting effect on magnetohydrodynamic (MHD) laminar and HT motion *via* the moving surface by the applied lie group method. Das [5] discussed the mathematical model of MHD motion of HT from electrically conducting liquid *via* parallel melting surface. Recently, Harish Babu *et al.* [6] explored the melting technology applied to magneto-NF motion *via* non-linear stretching surface. Venkateswarlu *et al.* [7] investigated numerical analysis of viscous dissipation and heat source on MHD motion *via* melting surface. Hayat *et al.* [8] explored the melting HT on 3D motion of NFs *via* impermeable SS. The melting HT and heat absorption characteristics in radiated stagnation point (SP) motion of Carreau liquid were created by Khan *et al.* [9]. The melting HT on MHD motion of Sisko liquid *via* nonlinear stretching velocity was examined by Hayat *et al.* [10]. Sheikholeslami and Rokni [11] presented the Buongiorno model that is applied to NF motion *via* stretching plate with magnetic field. Hayat *et al.* [12] explained the MHD SP motion of Jeffrey material *via* nonlinear SS. The microstructure of selective laser melting-built China low activation martensitic steel plates was analysed by Huang *et al.* [13]. Hajabdollahi *et al.* [14] investigated the close contact melting process generated by rotation. Fauzi *et al.* [15] examined the effect of melting effect on mixed convection boundary layer (BL) motion past a vertical surface *via* non-Darcian porous medium. Sheikholeslami *et al.* [16] analysed the impact of melting HT on NF motion with Lorentz forces.

The new-generation researchers are interested in doing the liquid motion when CR (combination of heterogeneous reaction [HR] and homogeneous reaction) is present. The physical condition values mentioned in HR and homogeneous reaction depend on weight, shape, distribution, architectural, size, appearance, colours, income, radioactivity, disease, temperature, and so on. Homogeneous reaction is very simple in comparison with HRs because homogeneous reaction depends upon only one nature reacting species. But the HR depends upon the two or more than two distinct nature reacting species. The heat generation rate is transpiring in liquid, whereas HR is supported on some catalyst surfaces only. Homogeneous catalyst transpires in gaseous state, whereas heterogeneous catalyst chances in solid state. These reactions' major role applications of chemical reaction in industries (such as hydrometallurgical industry, atmospheric flows, fog disposition and dissipation, biochemical systems, combustion, catalysis, ceramics and polymer production, *etc.*). Recently, DelaRosa *et al.* [17] analysed the use of heterogeneous catalysts with sulfonic group in hydrolysis of cellulose. Muto *et al.* [18] developed the unsteady numerical simulation with a detailed CR mechanism. Hayat *et al.* [19] presented the third-grade NF motion *via* stretchable rotating disk. Sulochanaa *et al.* [20] found that the variable porosity parameter has tendency to enhance HMT rate. Naukkarinen and Sainio [21] developed the field of CR engineering using the virtual laboratory (VL) concept. Yang *et al.* [22] explored the 2D surface and semi-finite wedge instability of oblique detonation waves. Sambath *et al.* [23] considered the CR and thermal radiation (TR) effect on natural convective hydromagnetic motion of viscous liquid *via* vertical cone. Some of the CR model problems were analysed in previous studies [24–26]. The CR on unsteady MHD NFs motion *via* SS was studied by Tarakaramu and Satya Narayan [27]. Veera Krishna and Gangadhar Reddy [28] presented the unsteady MHD free convection in a BL motion *via* a porous moving vertical plate with CR. Bhatti *et al.* [29] examined the nonlinear TR and CR effects on 3D MHD motion of viscous NFs with gyrotactic microorganisms *via* stretching porous cylinder. Recently, some important works on fluid flow are highlighted in previous studies [30–35].

The impact of heat source mechanism is known as a good regulatory mechanism of HT. This mechanism has more significant effect on NF motion owing to its engineering applications (metal waste, spent nuclear fuel, reactor safety analysis, radioactive materials, fire, and combustion). Jain and Bohra [36] presented the entropy generation on MHD liquid motion and HT *via* stretching cylinder with slip regime. Qayyum *et al.* [37] examined the impact of buoyancy force on MHD SP motion of tangent hyperbolic NFs. Hosseinzadeh *et al.* [38] discussed the non-uniform generation or absorption of HT in NFs motion *via* porous stretching sheet (SS). Ahmed and Elshehabey [39] explained that the buoyancy-driven HT enhances NFs motion with heat generation or absorption effect. Kanchana and Zhao [40] introduced the nonlinear stability analyses of Rayleigh–Benard convection with internal heat source in NFs. Recently, the generation or absorption influence on 3D NF motion models was developed [41–44]. Some of authors [45–48] developed numerical study of entropy generation on NFs *via* stretching surface. Some other studies regarding material applications, mathematical modelling and techniques, fluid flow, HT rate, and nanomaterial are addressed as follows: fluid flow behaviour examination [49–51], thermal mechanics [52–54], first hidden-charm pent quark with strangeness [55], and material characteristics [56–58].

The main intention and objective of this study to determine the nonlinear TR on 3D NF motion *via* SS with the anisotropic slip and melting effect. The major motivation of this work is to incorporate NFs to enhance the thermal conductivity and to make efficient HT. Also, the model is developed for the evaluation of the behaviour of TR parameter, melting parameter, Prandtl number, Brownian motion parameter, and thermophoresis parameter. The BL thickness *via* SS is increasingly being used in mechanical and physical processes, boiling, solar energy, maritime processes, aeronautical, and constructions. Flow of liquid and HT across SS is used in many technical processes, including polymer extrusion, food, and paper processing, fiberglass manufacturing, plastic film stretching, wire drawing, and continuous casting. The primary goal of the ongoing research is to learn about the properties of TR of 3D NF motion.

2 Mathematical formulation

Let us assume that the melting effect on 3D MHD motion of NFs *via* linear SS $z_1 = 0$ with heat source and CR. As shown in Figure 1, assume that the Cartesian coordinate system (x_1, y_1, z_1) corresponding to velocity components (u_1, u_2, u_3) is examined. The nanoparticles (NPs) are taken on the linear stretching surface. The surface velocity is assumed to be constant $(U_1, V_1, 0)$. A constant magnetic field is applied in the direction of z_1. The liquid motion on surface will be determined by the potential flow assumed as (ref. [59]):

$$u_1 = a_1 x_1, \qquad u_2 = a_1 y_1, \qquad u_3 = -2a_1 z_1, \qquad p_1 = -\frac{\rho_f a_1^2}{2}(x_1^2 + y_1^2) + p_0,$$

As per the aforementioned liquid motion consideration, we can formulate the continuity, momentum, conservative, and energy equations, which are as follows (ref. [59]):

$$\frac{\partial u_1}{\partial x_1} + \frac{\partial u_2}{\partial y_1} + \frac{\partial u_3}{\partial z_1} = 0, \tag{1}$$

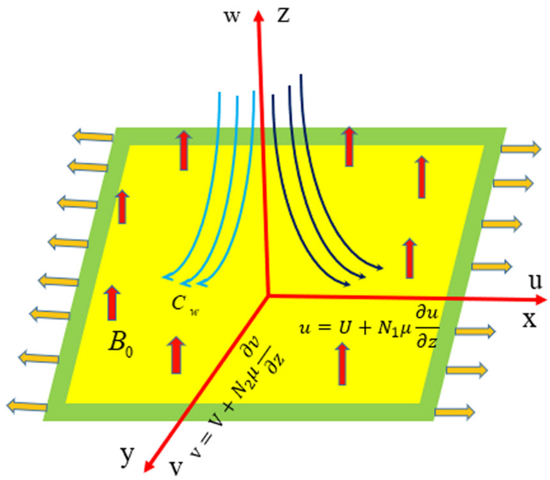

Figure 1: Physical model of the problem.

$$u_1\frac{\partial u_1}{\partial x_1} + u_2\frac{\partial u_1}{\partial y_1} + u_3\frac{\partial u_1}{\partial z_1} = -\frac{1}{\rho_f}\frac{\partial p_1}{\partial x_1} + \upsilon_1\left(\frac{\partial^2 u_1}{\partial {x_1}^2} + \frac{\partial^2 u_1}{\partial {y_1}^2} + \frac{\partial^2 u_1}{\partial {z_1}^2}\right) - \frac{\sigma_1 B_0^2}{\rho_f}u_1, \tag{2}$$

$$u_1\frac{\partial u_2}{\partial x_1} + u_2\frac{\partial u_2}{\partial y_1} + u_3\frac{\partial u_2}{\partial z_1} = -\frac{1}{\rho_f}\frac{\partial p_1}{\partial y_1} + \upsilon_1\left(\frac{\partial^2 u_2}{\partial {x_1}^2} + \frac{\partial^2 u_2}{\partial {y_1}^2} + \frac{\partial^2 u_2}{\partial {z_1}^2}\right) - \frac{\sigma_1 B_0^2}{\rho_f}u_2, \tag{3}$$

$$u_1\frac{\partial u_3}{\partial x_1} + u_2\frac{\partial u_3}{\partial y_1} + u_3\frac{\partial u_3}{\partial z_1} = -\frac{1}{\rho_f}\frac{\partial p_1}{\partial z_1} + \upsilon_1\left(\frac{\partial^2 u_3}{\partial {x_1}^2} + \frac{\partial^2 u_3}{\partial {y_1}^2} + \frac{\partial^2 u_3}{\partial {z_1}^2}\right) - \frac{\sigma_1 B_0^2}{\rho_f}u_3, \tag{4}$$

$$\left.\begin{array}{l} u_1\frac{\partial T_1}{\partial x_1} + u_2\frac{\partial T_1}{\partial y_1} + u_3\frac{\partial T_1}{\partial z_1} = \alpha_1\left(\frac{\partial^2 T_1}{\partial {x_1}^2} + \frac{\partial^2 T_1}{\partial {y_1}^2} + \frac{\partial^2 T_1}{\partial {z_1}^2}\right) \\ + \tau_1 D_B\left(\frac{\partial C_1}{\partial x_1}\frac{\partial T_1}{\partial x_1} + \frac{\partial C_1}{\partial y_1}\frac{\partial T_1}{\partial y_1} + \frac{\partial C_1}{\partial z_1}\frac{\partial T_1}{\partial z_1}\right) \\ + \frac{\tau_1 D_T}{T_\infty}\left(\left(\frac{\partial T_1}{\partial x_1}\right)^2 + \left(\frac{\partial T_1}{\partial y_1}\right)^2 + \left(\frac{\partial T_1}{\partial z_1}\right)^2\right) \\ - \frac{Q_0(T_1 - T_\infty)}{(\rho c_p)_f} - \frac{1}{(\rho c_p)}\frac{\partial q_r}{\partial z_1} \end{array}\right\}, \tag{5}$$

$$u_1\frac{\partial C_1}{\partial x_1} + u_2\frac{\partial C_1}{\partial y_1} + u_3\frac{\partial C_1}{\partial z_1} = D_B\left(\frac{\partial^2 C_1}{\partial {x_1}^2} + \frac{\partial^2 C_1}{\partial {y_1}^2} + \frac{\partial^2 C_1}{\partial {z_1}^2}\right) + \frac{D_T}{T_\infty}\left(\frac{\partial^2 T_1}{\partial {x_1}^2} + \frac{\partial^2 T_1}{\partial {y_1}^2} + \frac{\partial^2 T_1}{\partial {z_1}^2}\right) - k_0(C_1 - C_\infty). \tag{6}$$

Subject to boundary conditions are the anisotropic slip-on moving surface, constant NP volume fraction, and constant surface temperature as follows:

$$\left.\begin{array}{l} \left.\begin{array}{l} u_1 - U = N_1\mu_1\frac{\partial u_1}{\partial z_1},\ u_2 - V = N_2\mu_1\frac{\partial u_2}{\partial z}, \\ u_3 = 0\ \ T_1 = T_w,\ C = C_w, \\ k_1\left(\frac{\partial T_1}{\partial z_1}\right)_{z_1=0} = \rho(\lambda + c_s(T_m - T_s))u_2(x, 0) \end{array}\right\},\ \text{at } z_1 \to 0 \\ u_1 = a_1 x_1,\ u_2 = a_1 y_1,\ u_3 = -2a_1 z_1,\ T_1 = T_\infty,\ C_1 = C_\infty, \\ \text{as } {}_1z \to \infty \end{array}\right\}. \tag{7}$$

According to (ref. [60]), the radiative heat flux q_r is given by:

$$q_r = -\frac{4\sigma_1}{3k_1}\frac{\partial {T_1}^4}{\partial y_1}. \tag{8}$$

The temperature differences within motion are as follows:

$${T_1}^4 = T_\infty^4 + 4T_\infty^3(T_1 - T_\infty) + 6T_\infty^2(T_1 - T_\infty)^3 + \ldots \tag{9}$$

Now, by removing the higher-order terms beyond the first degree in $(T_1 - T_\infty)$, then

$${T_1}^4 = 4T_\infty^3 T_1 - 3T_\infty^4. \tag{10}$$

Solving Eq. (8) using Eq. (10), it can be transformed as follows:

$$\frac{\partial q_r}{\partial z_1} = -\frac{4\sigma_1 T_\infty^3}{3k_1}\frac{\partial^2 T_1}{\partial {z_1}^2}. \tag{11}$$

Therefore, using Eq. (11), then the energy Eq. (5) becomes

$$\left.\begin{array}{l} u_1\frac{\partial T_1}{\partial x_1} + u_2\frac{\partial T_1}{\partial y_1} + u_3\frac{\partial T_1}{\partial z_1} = \left(\alpha_1\left(\frac{\partial^2 T_1}{\partial {x_1}^2} + \frac{\partial^2 T_1}{\partial {y_1}^2} + \frac{\partial^2 T_1}{\partial {z_1}^2}\right)\right. \\ \left. + \frac{16\sigma_1 T_\infty^3}{3(\rho c_p)k_1}\frac{\partial q_r}{\partial z_1}\right)\frac{\partial^2 T_1}{\partial {z_1}^2} - \frac{Q_0(T_1 - T_\infty)}{(\rho c_p)} \\ + \tau_1 D_B\left(\frac{\partial C_1}{\partial x_1}\frac{\partial T_1}{\partial x_1} + \frac{\partial C_1}{\partial y_1}\frac{\partial T_1}{\partial y_1} + \frac{\partial C_1}{\partial z_1}\frac{\partial T_1}{\partial z_1}\right) \\ + \frac{\tau_1 D_T}{T_\infty}\left(\left(\frac{\partial T_1}{\partial x_1}\right)^2 + \left(\frac{\partial T_1}{\partial y_1}\right)^2 + \left(\frac{\partial T_1}{\partial z_1}\right)^2\right) \end{array}\right\}. \tag{12}$$

The suitable similarity variable is as follows:

$$\begin{array}{l} u_1 = a_1\, x_1\, f'(\eta),\ u_2 = a_1\, y_1\, g'(\eta), \\ u_3 = -\sqrt{a_1\upsilon_1}(f(\eta) + g(\eta)), \\ \eta = \sqrt{\frac{a_1}{\upsilon_1}}z_1,\ \theta(\eta) = \frac{T_1 - T_\infty}{T_f - T_\infty},\ \phi(\eta) = \frac{C_1 - C_\infty}{C_f - C_\infty}. \end{array} \tag{13}$$

Eqs. (2)–(4), (6), and (12) takes the following following form after implementing Eq. 13, we have

$$f''' = Mf' - f''(f+g) + (f')^2 - 1, \tag{14}$$

$$g''' = (g')^2 + g'M - g''(f+g) - 1, \tag{15}$$

$$\theta''(1+R_d) + \Pr(\theta'(f+g) + N_b\theta'\phi' + N_t(\theta')^2 - H\theta) = 0, \tag{16}$$

$$\phi'' = \gamma\phi - \mathrm{Le}\,\Pr(f+g)\,\phi' - \frac{N_t}{N_b}\theta''. \tag{17}$$

The converted boundary conditions are

$$\left.\begin{array}{l} \left.\begin{array}{l} f'(0) - \lambda_1 f''(0) = 0,\ g(0) = 0, \\ g'(0) - \lambda_2 g''(0) = 0 \\ \theta(0) = 1,\ \Pr f = -H\theta',\ \phi'(0) = 0 \end{array}\right\},\ \text{as } \eta \to 0 \\ f'(\infty) = 1,\ g'(\infty) = 1,\ \theta(\infty) = 0,\ \phi(\infty) = 0,\ \text{at } \eta \to \infty \end{array}\right\} \tag{18}$$

.

In some of physical important quantities in this work, *via* x_1- and y_1-directions of local Nusselt number Nu_{x_1} and Nu_{y_1}, local skin friction C_{fx_1} and C_{fy_1}. It is defined as:

$$\mathrm{Nu}_{x_1} = \frac{x_1 q_{u_3}}{k_1(T_w - T_\infty)},\ C_{fx_1} = \frac{\tau_{u_3x_1}}{\rho_f U^2}, \quad \mathrm{Nu}_{y_1} = \frac{y_1 q_{u_3}}{k_1(T_w - T_\infty)},\ C_{fy_1} = \frac{\tau_{u_3y_1}}{\rho_f V^2}, \tag{19}$$

where $\tau_{u_3x_1} = \mu_1\left(\frac{\partial u_1}{\partial z_1}\right)_{z_1=0},\ \tau_{u_3y_1} = \mu_1\left(\frac{\partial u_2}{\partial z_1}\right)_{z_1=0},\ q_m = -k_1\left(\frac{\partial T_1}{\partial z_1}\right)_{z_1=0}$.

Substituting Eqs. (13) into Eq. (19), we obtain

$$\mathrm{Re}_{x_1}^{-1/2}\mathrm{Nu}_{x_1} = -(1+R_d)\theta'(0), \quad \mathrm{Re}_{x_1}^{-1/2}C_{fx_1} = -f''(0),\ \mathrm{Re}_{y_1}^{-1/2}C_{fy_1} = -g''(0), \tag{20}$$

where the local Reynolds numbers $\mathrm{Re}_{x_1} = a_1 x_1^2/u_2$ and $\mathrm{Re}_{y_1} = a_1 y_1^2/u_2$ are along x_1- and y_1-directions, respectively.

2.1 Numerical analysis

Using shooting technique to solve the nonlinear system of Eqs. (14)–(17). To obtain a numerical solution by selecting a step size $\Delta\eta = 0.001$, we consider the momentum equation in the x and y directions, as well as the energy equations of third and second order, respectively. Momentum equation in the direction of x and y, energy equations are third and second order, respectively:

$$f''' = Mf' - f''(f+g) + (f')^2 - 1, \tag{21}$$

$$g''' = (g')^2 + g'M - g''(f+g) - 1, \tag{22}$$

$$\theta'' = (-\Pr/(1+R_d))(\theta'(f+g) + N_b\theta'\phi' + N_t(\theta')^2 - H\theta), \tag{23}$$

$$\phi'' = \gamma\phi - \mathrm{Le}\,\Pr(f+g)\,\phi' - \frac{N_t}{N_b}\theta''. \tag{24}$$

Considering dependent variables $\xi_1,\ \xi_2,\ \xi_3,\ \xi_4,\ \xi_5,\ \xi_6,\ \xi_7,\ \xi_8,\ \xi_9,\ \xi_{10},\ \xi_{12}$, and ξ_{13} and substituting in Eqs. (21)–(24), then we obtain the following format:

$$f = \xi_1, \tag{25}$$

$$f' = \xi_2' = \xi_2, \tag{26}$$

$$f'' = \xi_3' = \xi_3, \tag{27}$$

$$f''' = \xi_4' = \xi_4 = M\xi_2 - \xi_4(\xi_1 + \xi_5) + (\xi_2)^2 - 1, \tag{28}$$

$$g = \xi_5, \tag{29}$$

$$g' = \xi_6' = \xi_6, \tag{30}$$

$$g'' = \xi_7' = \xi_7, \tag{31}$$

$$g''' = \xi_8' = \xi_8 = (\xi_6)^2 - (\xi_1 + \xi_5)\,\xi_7 - 1, \tag{32}$$

$$\theta = \xi_9' = \xi_9, \tag{33}$$

$$\theta' = \xi_{10}' = \xi_{10}, \tag{34}$$

$$\theta'' = \xi_{11}' = \xi_{11} = (-\Pr/(1+R_d))(\xi_{10}(\xi_1 + \xi_5) + N_b\xi_{10}\xi_{12} + N_t(\xi_{10})^2 - H\xi_9), \tag{35}$$

$$\phi = z_{11}' = z_{11}, \tag{36}$$

$$\phi' = z_{12}' = z_{12}, \tag{37}$$

$$\phi'' = \xi_{13} = \gamma\xi_{11} - \mathrm{Le}\,\Pr(f+g)\,\xi_{12} - \frac{N_t}{N_b}((-\Pr/(1+R_d))(\xi_{10}(\xi_1+\xi_5) + N_b\xi_{10}\xi_{12} + N_t(\xi_{10})^2 - H\xi_9)). \tag{38}$$

Associated boundary layer as formated below

$$\left.\begin{array}{l} \left.\begin{array}{l} f'(0) - \lambda_1 f''(0) = 0,\ g(0) = 0, \\ g'(0) - \lambda_2 g''(0) = 0 \\ \theta(0) = 1,\ \Pr f = -H\theta',\ \phi'(0) = 0 \end{array}\right\},\ \text{as } \eta \to 0 \\ f'(\infty) = 1,\ g'(\infty) = 1,\ \theta(\infty) = 0,\ \phi(\infty) = 0, \\ \text{at } \eta \to \infty \end{array}\right\}. \tag{39}$$

To solve system of Eqs. (21)–(25) ten initial conditions must be known, but ξ_4, ξ_8, ξ_{11}, and ξ_{13} are unknown, at $\zeta \to \infty$, boundary condition of $f(\zeta)$, $g(\zeta)$, $\theta(\zeta)$, $\phi(\zeta)$ are unknown, and these three unknown conditions are indicated by ξ_1, ξ_5, ξ_9, and ξ_{11}. In order to achieve an error of less than 10^{-10}, the parameters taken must be approximated to a finite value, denoted as ζ_∞, using Newton's scheme.

3 Results and discussion

The variation of M (magnetic field parameter) on $f'(\eta)$ and $g'(\eta)$ is presented in Figure 2. It is seen that the $f'(\eta)$ and $g'(\eta)$ declined with various statistical values of M. Furthermore, a variation of relative study reveals that $\mathrm{Re}_x^{1/2}C_{fx}$ (skin friction coefficient *via* axial direction) decays with various distinct values of Mt (Melting parameter) against λ_1 (slip parameter *via* x_1-axis) for both cases $M = 0$ and $M > 0$, as explored in Figure 3. It is noted that the hydrodynamic ($M = 0$) is lower than the hydromagnetic case ($M > 0$) along x_1-direction. Physically, M is direct proportional to EC (electrical conductivity); due to this, the magnetic field and resistive force applied act more into opposite direction of liquid motion, and low EC, and then liquid speed goes to very slow motion in stretching surface.

Figure 4 presents the effect of Mt (melting parameter) on $\theta(\eta)$ (temperature profile). It is noted that the $\theta(\eta)$ dwindles with distinct statistical values of Mt. Physically, the melting parameter is a combination of Stefan numbers for solid and liquid aspects. Also, it is proportional to specific heat at constant pressure. Due to this fact, the fluid particles yield low temperature.

The influence of R_d (TR parameter) on $\theta(\eta)$ is shown in Figure 5a. It is noted that $\theta(\eta)$ improves with distinct statistical values of R_d, while the reverse behaviour follows concentration as predicted in Figure 5b. Physically, the TR is inversely proportional to TD (thermal diffusivity); due to this, the low TD in liquid motion at stretching surface released high temperature and low concentration.

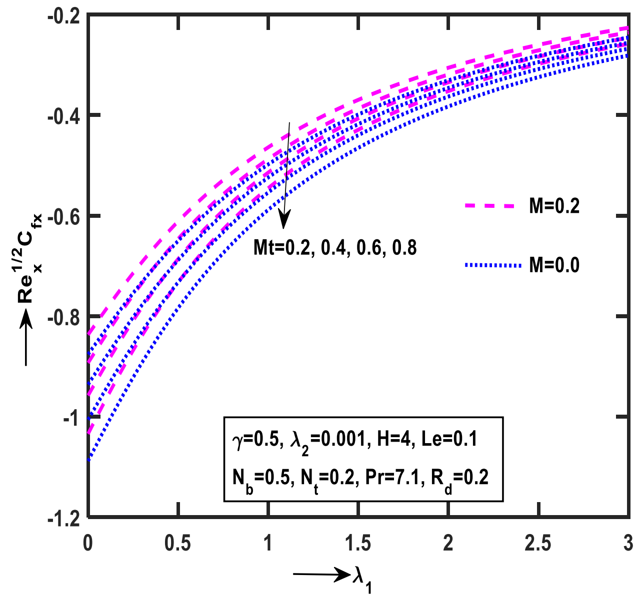

Figure 3: Impact of Mt on $\mathrm{Re}_x^{1/2}C_{fx}$.

The variation of Pr (Prandtl number) on $\theta(\eta)$ is shown in Figure 6. As expected, thermal BL decays for different statistical values of Pr. Physically, Pr is inversely proportional to TD. Due to this, the TD released low temperature in NF motion at surface area.

Figure 7 indicates the behaviour of N_t (thermophoresis parameter) on $\theta(\eta)$. It is seen that the thermal BL converges high in region $1 \le \eta \le 0.8$ (approximate region) with ascending statistical values of N_t, whereas the opposite behaviour displays N_b (Brownian motion parameter),

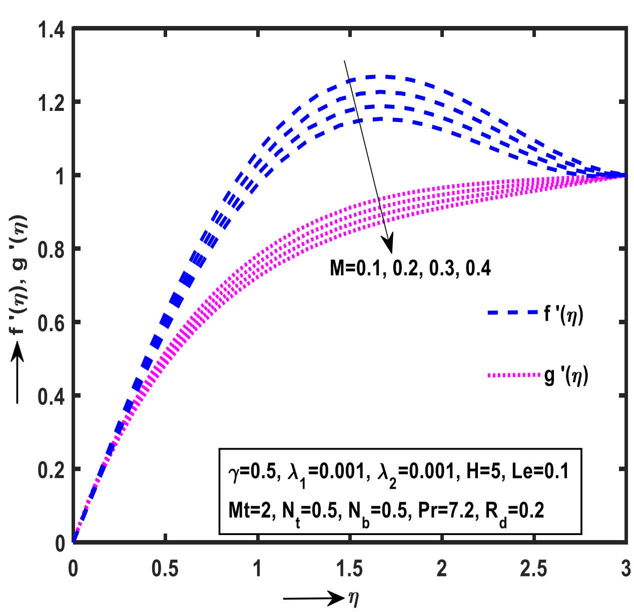

Figure 2: Impact of M on $f'(\eta)$ and $g'(\eta)$.

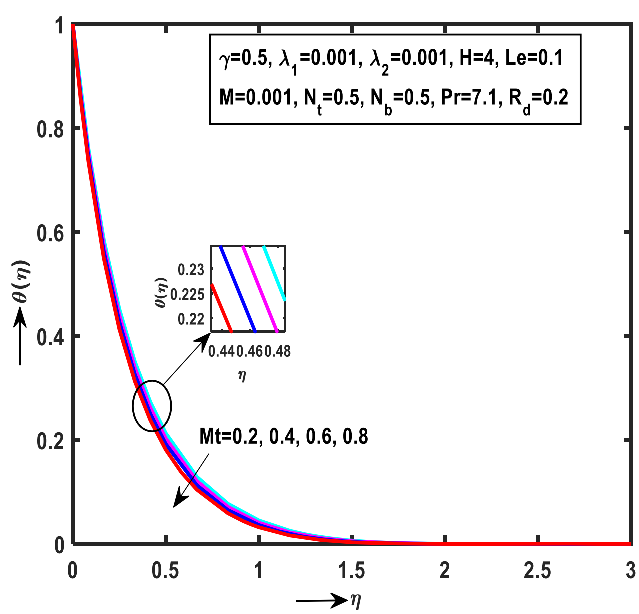

Figure 4: Impact of Mt on $\theta(\eta)$.

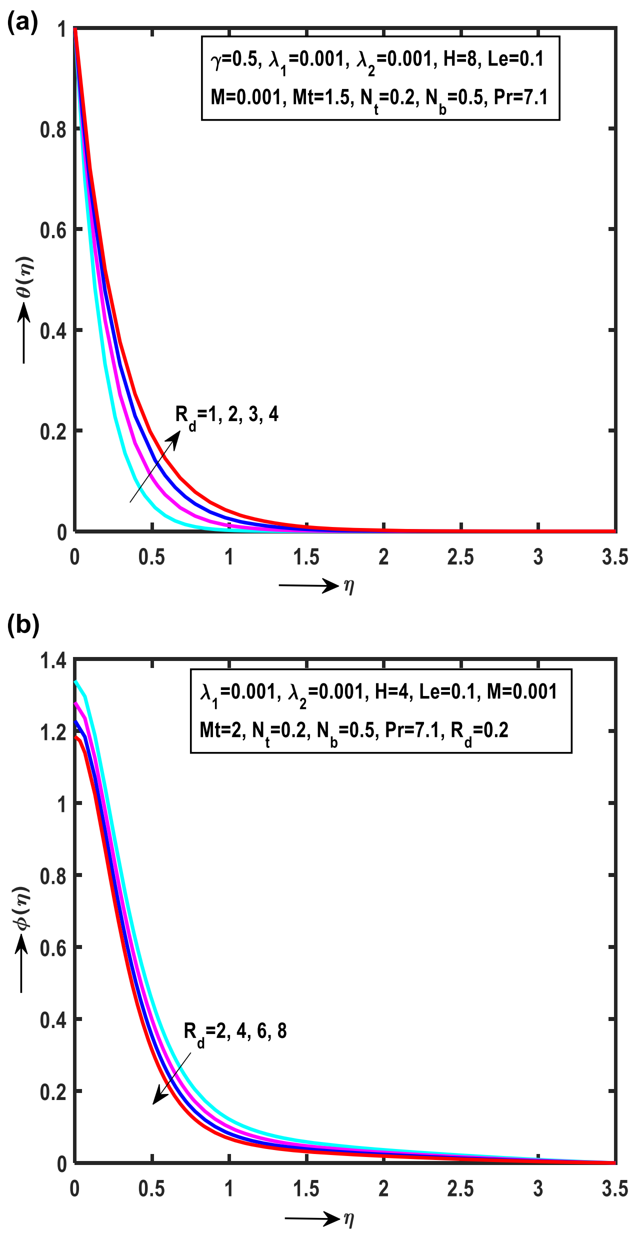

Figure 5: (a) Impact of R_d on $\theta(\eta)$. (b) Impact of R_d on $\phi(\eta)$.

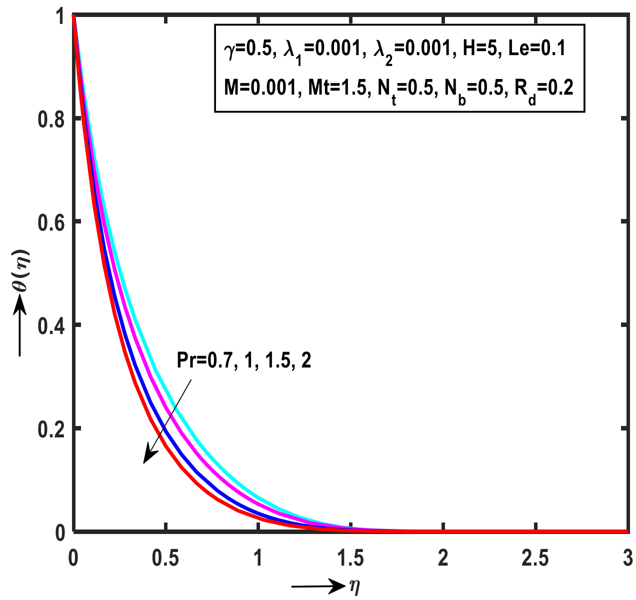

Figure 6: Impact of Pr on $\theta(\eta)$.

as shown in Figure 8. Physically, the Brownian motion and thermophoresis parameters are inversely proportional to kinematic viscosity. The kinematic viscosity released high temperature in NF motion at SS.

Figure 9 shows the effect of Le (Lewis number) on $\phi(\eta)$ (concentration profile). It is observed that the low concentration BL for ascending numerical values of Le. Physically, the Lewis number is ratio of TD to Brownian diffusivity. The low TD released low concentration in motion of NFs.

The impact of λ_1 (slip parameter *via* axial direction direction) and λ_2 (slip parameter *via* transverse direction) on $Re_x^{1/2}C_{fy}$ is shown in Figure 10. It is clear that the skin friction enhances along the y_1-direction for enlarged values of λ_1. Physically, the slip factor is proportional to dynamic viscosity. NFs with low dynamic viscosity produce low coefficient of skin friction at SS.

Figure 11 presents the behaviour of NFs and RFs (regular fluids) with various ascending values of H (heat source parameter) against λ_1 on the HT rate. It is observed that the $Re_x^{-1/2}Nu_x$ declined for distinct ascending statistical values of H. It is also stated that the high HT rate is reduced in case of NFs when compared to RF motion.

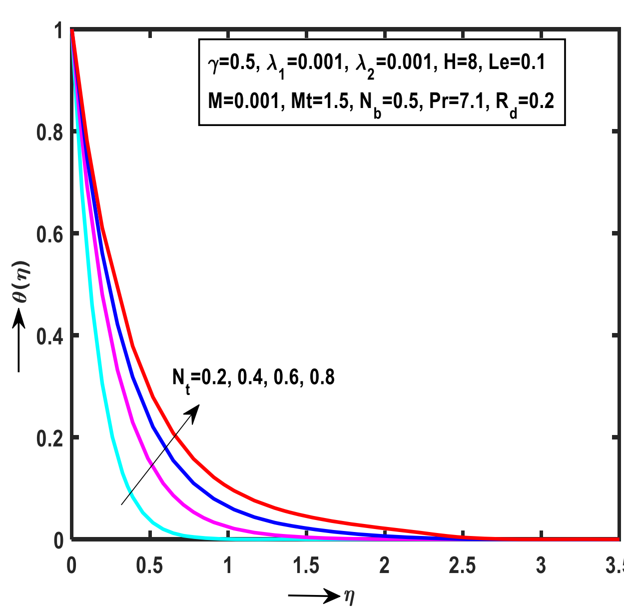

Figure 7: Impact of N_t on $\theta(\eta)$.

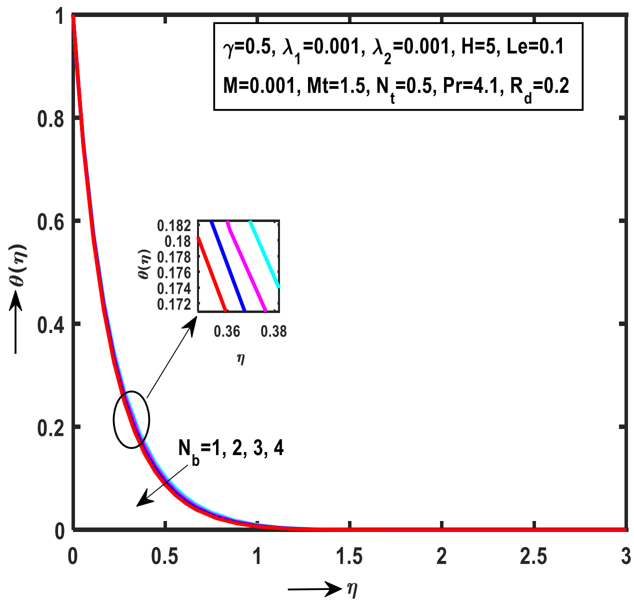

Figure 8: Impact of N_b on $\theta(\eta)$.

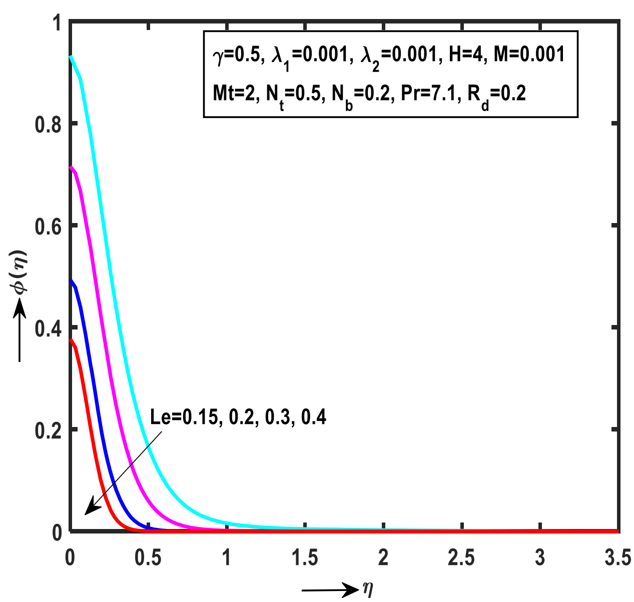

Figure 9: Impact of Le on $\phi(\eta)$.

4 Conclusion

This study provides valuable insights into the behaviour of NFs in terms of liquid motion and HT. The findings can be used to optimize the design and performance of systems involving NFs, and to enhance the efficiency of processes such as boiling, solar energy utilization, and micro power generation. The results highlight the importance of considering factors such as slip influence, magnetic field, and chemical reactions in the analysis of NF behaviour. The

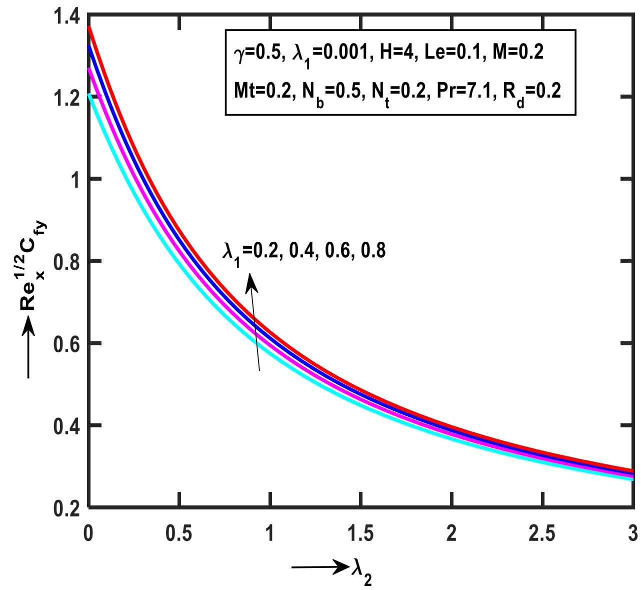

Figure 10: Impact of λ_1 on $\mathrm{Re}_x^{1/2}C_{fy}$.

findings also emphasize the potential of NFs to significantly enhance heat transfer compared to regular liquids. Further research can build upon these findings to explore additional parameters and conditions, and to develop more accurate and comprehensive models for NF behaviour. Overall, this research contributes to the understanding and advancement of NF technology, opening up new possibilities for its application in various engineering fields. The main results are mentioned as follows:

- The $f'(\eta)$ and $g'(\eta)$ decrease for distinct enlarged statistical values of M. On the other hand, the $\mathrm{Re}_x^{1/2}C_{fx}$ decays along the x_1-direction with various ascending values of Mt for the cases of $M = 0$ and $M > 0$.

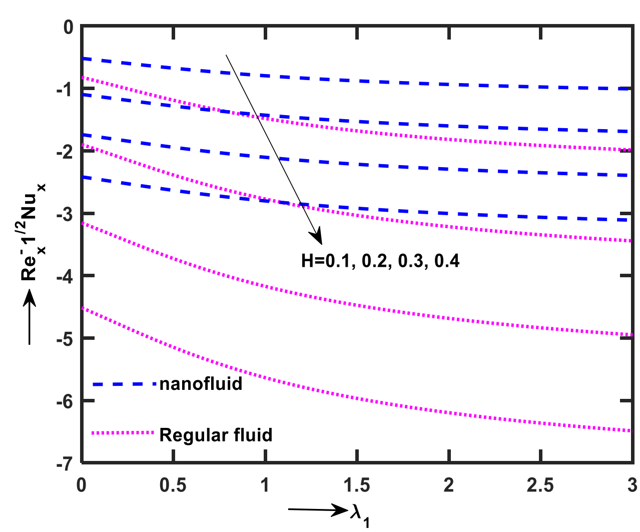

Figure 11: Impact of H on $\mathrm{Re}_x^{1/2}\mathrm{Nu}_x$.

- The $\mathrm{Re}_x^{1/2} C_{fy}$ enhances along the y_1-direction with distinct enlarged values of λ_1 against λ_2
- The variation of $\mathrm{Re}_x^{1/2} \mathrm{Nu}_x$ decreases for the cases of NFs and RFs with distinct enlarged values of H.

Acknowledgments: The authors express their gratitude to Princess Nourah bint Abdulrahman University Researchers Supporting Project (Grant No. PNURSP2024R12), Princess Nourah bint Abdulrahman University, Riyadh, Saudi Arabia.

Funding information: The authors state no funding involved.

Author contributions: All authors have accepted responsibility for the entire content of this manuscript and approved its submission.

Conflict of interest: The authors state no conflict of interest.

References

[1] Epstein M, Cho DH. Melting heat transfer in steady laminar flow over a flat plate. ASME J Heat Mass Transf. 1976;98(3):531–3.

[2] Kazmierczak M, Poulikakos D, Sadowski D. Melting of a vertical plate in porous medium controlled by forced convection of a dissimilar fluid. Int Commun Heat Mass Transf. 1987;14:507–17.

[3] Kazmierczak M, Poulikakos D, Pop I. Melting from a flat plate in a porous medium in the presence of steady convection. Numer Heat Transf. 1986;10:571–81.

[4] Rahman RGA, Khader MM, Megahed AM. Melting phenomenon in magneto hydro-dynamics steady flow and heat transfer over a moving surface in the presence of thermal radiation. Chin Phys B. 2013;22(3):030202.

[5] Das K. Radiation and melting effects on MHD boundary layer flow over a moving surface. Ain Shams Eng J. 2014;5:1207–14.

[6] Harish Babu D, Harinath Reddy S, Kumaraswamy Naidu K, Sathya Narayana PV, Venkateswarlu B. Numerical investigation for entropy-based magneto nanofluid flow over non-linear stretching surface with slip and convective boundary conditions. 2023;103(10):e202300006. doi: 10.1002/zamm.202300006.

[7] Venkateswarlu B, Satya Narayana PV, Tarakaramu N. Melting and viscous dissipation effects on MHD flow over a moving surface with constant heat source. Trans A Razmadze Math Inst. 2018;172(3):619–30.

[8] Hayat T, Muhammad K, Alsaedi A, Asghar S. Numerical study for melting heat transfer and homogeneous heterogeneous reactions in flow involving carbon nanotubes. Results Phys. 2018;8:415–21.

[9] Khan MI, Waqas M, Hayat T, Khan MI, Alsaedi A. Melting heat transfer in stagnation point of Carreau fluid with nonlinear thermal radiation and heat source. J Braz Soc Mech Sci Eng. 2018;40:270.

[10] Hayat T, Ullah I, Alsaedi A, Asghar S. Magnetohydrodynamics stagnation-point flow of Sisko liquid with melting heat transfer and heat generation/absorption. J Therm Sci Eng Appl. 2018;10:1–8. doi: 10.1115/1.4040032.

[11] Sheikholeslami M and Rokni HB. Effect of melting heat transfer on nanofluid flow in existence of magnetic field considering Buongiorno Model. Chin J Phys. 2017;55:1115–26.

[12] Hayat T, Saif RS, Ellahi R, Muhammad T, Alsaedi A. Simultaneous effects of melting heat and internal heat generation in stagnation point flow of Jeffrey fluid towards a nonlinear stretching surface with variable thickness. Int J Therm Sci. 2018;132:344–54.

[13] Huang B, Zhai Y, Liu S, Mao X. Microstructure anisotropy and its effect on mechanical properties of reduced activation ferritic/martensitic steel fabricated by selective laser melting. J Nucl Mater. 2018;500:33–41.

[14] Hajabdollahi F, Premnath KN, Malepati S. Effects of the magnetic field on direct contact melting transport processes during rotation. Appl Math Model. 2018;61:42–442.

[15] Fauzi NF, Merkin JH, Ahmad S, Pop I. The mixed convection boundary layer on a vertical melting front in a non-Darcian porous medium. Transp Porous Med. 2017;116:521–32. doi: 10.1007/s11242-016-0788-6.

[16] Sheikholeslami M, Nimafar M, Ganji DD. Analytical approach for the effect of melting heat transfer on nanofluid heat transfer. Eur Phys J Plus. 2017;132(385):1–12.

[17] DelaRosa SM, Martin JMC, Fierro JLG. Chemical hydrolysis of cellulose into fermentable sugars through ionic liquids and antisolvent pre-treatments using heterogeneous catalysts. Catal Today. 2018;302:87–93.

[18] Muto M, Yuasa K, Kurose R. Numerical simulation of soot formation in pulverized coal combustion with detailed chemical reaction mechanism. Adv Powder Technol. 2018;29:1119–27.

[19] Hayat T, Ahmad S, Khan MI, Alsaedi A. Modeling and analysing flow of third grade nanofluid due to rotating stretchable disk with chemical reaction and heat source. Phys B: Condens Matter. 2018;537:116–26.

[20] Sulochanaa C, Samrata SP, Sandeep N. Numerical investigation of magnetohydrodynamic (MHD) radiative flow over a rotating cone in the presence of Soret and chemical reaction. Propuls Power Res. 2018;7(1):91–101.

[21] Naukkarinen J, Sainio T. Supporting student learning of chemical reaction engineering using a socially scaffolded virtual laboratory concept. Educ Chem Eng. 2018;22:61–8.

[22] Yang P, Teng H, Ng HD, Jiang Z. A numerical study on the instability of oblique detonation waves with a two-step induction-reaction kinetic model. Proc Combust Inst. 2019;37(3):3537–44.

[23] Sambath P, Pullepu B, Hussain T, Shehzad SA. Radiated chemical reaction impacts on natural convective MHD mass transfer flow induced by a vertical cone. Results Phys. 2018;8:304–15.

[24] Khan M, Irfan M, Khan WA. Thermophysical properties of unsteady 3D flow of magneto Carreau fluid in the presence of chemical species: a numerical approach. J Braz Soc Mech Sci Eng. 2018;40(108):1–15. doi: 10.1007/s40430-018-0964-4.

[25] Mozgunov P, Beccuti M, Horvath A, Jaki T, Sirovich R, Bibbona E. A review of the deterministic and diffusion approximations for stochastic chemical reaction networks. React Kinet Mech Catal. 2018;128:289–312. doi: 10.1007/s11144-018-1351-y.

[26] Yang W, Wang Y. Analysis on stability and non-existence of equilibrium for a general chemical reaction. Electron J Qual Theory Differ Equ. 2018;17:1–12. doi: 10.14232/ejqtde.2018.1.17.

[27] Tarakaramu N, Satya Narayan PV. Unsteady MHD nanofluid flow over a stretching sheet with chemical reaction. IOP Conf Ser: Mater Sci Eng. 2017;263:1–8. doi: 10.1088/1757-899X/263/6/062030.

[28] Veera Krishna M, Gangadhar Reddy M. MHD free convective boundary layer flow through porous medium past a moving vertical plate with heat source and chemical reaction. Mater Today: Proc. 2018;5:91–8.
[29] Bhatti MM, Mishra SR, Abbas T, Rashidi MM. A mathematical model of MHD nanofluid flow having gyrotactic microorganisms with thermal radiation and chemical reaction effects. Neural Comput Appl. 2018;30:1237–49. doi: 10.1007/s00521-016-2768-8.
[30] Li S, Ali F, Zaib A, Loganathan K, Eldin SM, Khan MI. Bioconvection effect in the Carreau nanofluid with Cattaneo–Christov heat flux using stagnation point flow in the entropy generation: Micromachines level study. Open Phys. 2023;21:20220228.
[31] Li S, Khan MI, Alzahrani F, Eldin SM. Heat and mass transport analysis in radiative time dependent flow in the presence of Ohmic heating and chemical reaction, viscous dissipation: An entropy modeling. Case Stud Therm Eng. 2023;42:102722.
[32] Li S, Puneeth V, Saeed AM, Singhal A, Al-Yarimi FAM, Khan MI, et al. Analysis of the Thomson and Troian velocity slip for the flow of ternary nanofluid past a stretching sheet. Sci Rep. 2023;13:2340.
[33] Liu Z, Li S, Sadaf T, Khan SU, Alzahrani F, Khan MI, et al. Numerical bio-convective assessment for rate type nanofluid influenced by Nield thermal constraints and distinct slip features. Case Stud Therm Eng. 2023;44:102821.
[34] Li S, Raghunath K, Alfaleh A, Ali F, Zaib A, Khan MI, et al. Effects of activation energy and chemical reaction on unsteady MHD dissipative Darcy-Forcheimer squeezed flow of Casson fluid over horizontal channel. Sci Rep. 2023;13:2666.
[35] Chu YM, Khan MI, Abbas T, Sidi MO, Alharbi KAM, Alqsair UF, et al. Radiative thermal analysis for four types of hybrid nanoparticles subject to non-uniform heat source: Keller box numerical approach. Case Stud Therm Eng. 2022;40:102474.
[36] Jain S, Bohra S. Entropy generation on MHD slip flow over a stretching cylinder with heat generation/absorption. Int J Appl Mech Eng. 2018;23(2):413–28. doi: 10.2478/ijame-2018-0024.
[37] Qayyum S, Hayat T, Shehzad SA, Alsaedi A. Mixed convection and heat generation/absorption aspects in MHD flow of tangent-hyperbolic nanoliquid with Newtonian heat/mass transfer. Radiat Phys Chem. 2018;144:396–404.
[38] Hosseinzadeh KH, Afsharpanah F, Zamani S, Gholinia M, Ganji DD. A numerical investigation on ethylene glycol-titanium dioxide nanofluid convective flow over a stretching sheet in presence of heat generation/absorption. Case Stud Therm Eng. 2018;12:228–36.
[39] Ahmed SE, Elshehabey HM. Buoyancy-driven flow of nanofluids in an inclined enclosure containing an adiabatic obstacle with heat generation/absorption: Effects of periodic thermal conditions. Int J Heat Mass Transf. 2018;124:58–73.
[40] Kanchana C, Zhao Y. Effect of internal heat generation/absorption on Rayleigh-Bénard convection in water well-dispersed with nanoparticles or carbon nanotubes. Int J Heat Mass Transf. 2018;127:1031–47.
[41] Jagadeesh S, Chenna Krishna Reddy M, Tarakaramu N, Ahmad H, Askar S, Abdullaev SS. Convective heat and mass transfer rate on 3D Williamson nanofluid flow via linear stretching sheet with thermal radiation and heat absorption. Sci Rep. 2023;13:9889.
[42] Wang F, Tarakaramu N, Govindaraju MV, Sivakumar N, Bhagya Lakshmi K, Satya Narayana PV, et al. Activation energy on three-dimensional Casson nanofluid motion via stretching sheet: Implementation of Buongiorno's model. J Indian Chem Soc. 2023;100886.
[43] Hayat T, Qayyum S, Alsaedi A, Ahmad B. Significant consequences of heat generation/absorption and homogeneous-heterogeneous reactions in second grade fluid due to rotating disk. Results Phys. 2018;8:223–30.
[44] Hussain Z, Hayat T, Alsaedi A, Ahmad B. Three-dimensional convective flow of CNTs nanofluids with heat generation/absorption effect: A numerical study. Comp Methods Appl Mech Eng. 2018;329:40–54.
[45] Harish Babu D, Sathya Narayana PV. Melting heat transfer and radiation effects on Jeffrey fluid flow over a continuously moving surface with a parallel free stream. J Appl Comput Mech. 2019;5(2):468–76.
[46] Tarakaramu N, Sivakumar N, Tamam N, Satya Narayana PV, Ramalingam S. Theoretical analysis of Arrhenius activation energy on 3D MHD nanofluid flow with convective boundary condition. Mod Phys Lett B. 2023;2341009. doi: 10.1142/S0217984923410099.
[47] Sathya Narayana PV, Harish Babu D, Sudheer Babu M. Numerical study of a Jeffrey fluid over a porous stretching sheet with heat source/sink. Int J Fluid Mech Res. 2019;4(2):187–97.
[48] Masthanaiah Y, Tarakaramu N, Ijaz Khan M, Rushikesava A, Moussa SB, Fadhi BM, et al. Impact of viscous dissipation and entropy generation on cold liquid via channel with porous medium by analytical analysis. Case Stud Therm Eng. 2023;47:103059.
[49] Xu J, Liu J, Zhang Z, Wu X. Spatial-temporal transformation for primary and secondary instabilities in weakly non-parallel shear flows. J Fluid Mech. 2023;959:A21.
[50] Zhu S, Li X, Bian Y, Dai N, Yong J, Hu Y, et al. Inclination-enabled generalized microfluid rectifiers via anisotropic slippery hollow tracks. Adv Mater Technol. 2023;8(16):2300267. doi: 10.1002/admt.202300267.
[51] Yang L, Wang H, Xu H, Guo D, Li M. Experimental study on characteristics of water imbibition and ion diffusion in shale reservoirs. Geoenergy Sci Eng. 2023;229:212167.
[52] Du S, Xie H, Yin J, Fang T, Zhang S, Sun Y, et al. Competition pathways of energy relaxation of hot electrons through coupling with optical, surface, and acoustic phonons. J Phys Chem C. 2023;127:1929–36.
[53] Wang J, Chong X, Lv L, Wang Y, Ji X, Yun H, et al. High-entropy ferroelastic (10RE0.1)TaO4 ceramics with oxygen vacancies and improved thermophysical properties. J Mater Sci Technol. 2023;157:98–106.
[54] Wang Z, Wang Q, Jia C, Bai J. Thermal evolution of chemical structure and mechanism of oil sands bitumen. Energy (Oxf). 2022;244:1. doi: 10.1016/j.energy.2022.123190.
[55] Chen H, Chen W, Liu X, Liu X. Establishing the first hidden-charm pentaquark with strangeness. Eur Phys J C. 2021;81:409.
[56] Liu W, Zhao C, Zhou Y, Xu X, Rakkesh RA. Modeling of vapor-liquid equilibrium for electrolyte solutions based on COSMO-RS interaction. J Chem. 2022;2022:9070055.
[57] He Y, Zhang L, Tong MS. Microwave imaging of 3D dielectric-magnetic penetrable objects based on integral equation method. IEEE Trans Antennas Propag. 2023;71(6):5110–20. doi: 10.1109/TAP.2023.3262299.
[58] Kong L, Liu G. Synchrotron-based infrared micro-spectroscopy under high pressure: An introduction. Matter Radit Extremes. 2021;6:68202.
[59] Raees A, Haq MRU, Xu H, Sun Q. Three-dimensional stagnation flow of a nanofluid containing both nanoparticles and microorganisms on a moving surface with anisotropic slip. Appl Math Model. 2016;40:4136–50.
[60] Brewster MQ. Thermal radiative transfer properties, General & Introductory. Mech Engineering/thermodynamic. 1992;568.